Constructing Love-Q relations with gravitational wave detections

Anuradha Samajdar[1,2] and Tim Dietrich[1,3]

[1]*Nikhef, Science Park 105, 1098 XG Amsterdam, Netherlands*
[2]*Department of Physics, Utrecht University, Princetonplein 1, 3584 CC Utrecht, Netherlands*
[3]*Institut für Physik und Astronomie, Universität Potsdam, Haus 28, Karl-Liebknecht-Str. 24/25, 14476, Potsdam, Germany*

(Received 24 February 2020; accepted 27 May 2020; published 9 June 2020)

Quasiuniversal relations between the tidal deformability and the quadrupole moment of neutron stars are predicted by theoretical computations, but have not been measured experimentally. We simulate 120 binary neutron star sources and find that Advanced LIGO and Advanced Virgo at design sensitivity could find possible deviations from predicted relations if the neutron stars are highly spinning. A network of envisaged third generation detectors will even allow extracting such relations, providing new tests of general relativity and nuclear physics predictions.

DOI: 10.1103/PhysRevD.101.124014

I. INTRODUCTION

The observation of GW170817 proved that gravitational waves (GWs) serve as a new observational window to probe matter at supranuclear densities and to decode the unknown equation of state (EOS) governing the neutron star's interior [1–3]. Already from this single detection, it was possible to place constraints on the supranuclear EOS, e.g., [1,2,4–13] and to disfavor some of the theoretical predictions. The recent detection of another binary neutron star (BNS) merger, GW190425 [14], however, does not shed additional light on EOS information because of its high mass [13,15,16]. Nevertheless, rate estimates for BNS coalescences (250–2810 $\mathrm{Gpc}^{-3}\,\mathrm{yr}^{-1}$ [14]) show that we can expect many more BNS signals to be detected in the near future.

During a BNS coalescence, each neutron star undergoes tidal deformation due to the influence of the other star's gravitational field. This tidal deformability is imprinted in the emitted GW signal and carries information about the internal structure of the star. The main quantity characterizing these tidal deformations is the tidal polarizability $\Lambda = 2k_2/(3C^5)$ with k_2 being the tidal Love number describing the static quadrupolar deformation of one neutron star in the gravitoelectric field of the companion and C being the compactnesses of the star at isolation.

In addition, a spinning neutron star undergoes deformation, encoded in an additional *spin-induced* quadrupole moment. For rotating neutron stars, the quadrupole moments vary as $\mathcal{Q} \simeq -Q\chi^2 m^3$ with χ and m being the dimensionless spin and the mass of the object; see [17,18] for discussions and Ref. [19] for an upgrade and update of [18]. Here, Q is a parameter connected to the internal structure of the neutron star depending on the supranuclear EOS. For a given EOS, this relation may be written as $\mathcal{Q} \simeq -Q(m)\chi^2$. The corresponding imprint in the GW phasing from $\mathcal{Q}$ was computed in [20]. References [21,22] laid out the importance of the quadrupole moment on the measurability of parameters in GW signals for highly spinning NSs and [23] investigated possible effects on GW signals introduced by the spin-induced quadrupole moments by combining information from multiple signals. Finally, [24] used the measurement of spin-induced quadrupole moments as a probe to distinguish between a binary black hole signal within general relativity and a signal arising from a binary of exotic compact objects. The analysis was further extended to a Bayesian approach in [25], the only work which samples directly on the spin-induced quadrupole moment parameters.

Most analyses performed on GW signals GW170817 and GW190425 inferred the quadrupole moment of each neutron star from their tidal deformabilities, by leaving the latter as free parameters and using the EOS-insensitive relations [2,3,14] to determine the spin-induced quadrupole moment. Quasiuniversal relations connecting the tidal deformability and the spin-induced quadrupole moment of neutron stars were first introduced by Yagi and Yunes [26] and have been improved by incorporating information from GW170817 [27]. While these EOS-insensitive relations are to second order in the slow-rotation approximation essentially independent of the NS spin, additional deviations may occur for fast rotating neutron stars [26]. Breakdown of these relations from fast rotations [28] as well as strong magnetic fields [29] has been explored. In addition, frequency-dependent nature of tidal deformability has been explored in [30] and the composition-dependent nature has been studied in [31]. We explore the spin-induced moments which enter at the early inspiral regime and consider the tidal deformability to be constant, as the

effects of frequency and composition dependence come into play in later stages of the inspiral and will likely not affect our analysis. However, we point out that these relations have been employed for the analysis of GW170817 and GW190425 even beyond the neutron star's breakup spin. Therefore, we want to ask the question whether it is possible to verify and potentially measure the relation between the quadrupole moment and the tidal deformability from real GW data. For this purpose, we use the Yagi-Yunes relation [26,32] that connects the quadrupole moment to the tidal deformability

$$\ln Q = a_i + b_i \ln \Lambda + c_i \ln \Lambda^2 + d_i \ln \Lambda^3 + e_i \ln \Lambda^4, \quad (1)$$

with the fitting parameters $a_i = 0.194$, $b_i = 0.0936$, $c_i = 0.0474$, $d_i = -4.21 \times 10^{-3}$, and $e_i = 1.23 \times 10^{-4}$. We use the quadrupole moments of the individual stars as free parameters and sample on them during the analysis instead of relying on the existing quasiuniversal relations to infer them from their corresponding tidal deformability parameters. While this increases the dimensionality of the problem and leads to larger uncertainties in the observed parameters, it also allows to test and find relations between the quadrupole moment and the tidal deformability.

II. METHODS

We perform a Bayesian analysis for parameter estimation using the LALInference module [33] available in the LALSuite [34] package. We employ the nested sampling algorithm to estimate posterior probability distribution functions [35,36] which further encode information about the parameters. The parameter set of a BNS source consists of $\{m_1, m_2, \chi_1, \chi_2, \theta, \phi, \iota, \psi, D_L, t_c, \varphi_c, \Lambda_1, \Lambda_2\}$. m_i is the mass of the ith object, $\chi_i = \frac{\vec{S}_i}{m_i^2} \cdot \hat{L}$ is the dimensionless spin parameter aligned with the direction of the orbital angular momentum $\hat{L}$, θ and ϕ are the angular coordinates denoting the sky location, ι and ψ are the angles describing the binary's orientation with respect to the line of sight, D_L is the luminosity distance to the source, t_c and φ_c are the time and phase at the instance of coalescence, and Λ_i are the dimensionless tidal deformability parameters. In addition, our parameter set also includes the spin-induced quadrupole moments $dQ_1 = Q_1 - 1$ and $dQ_2 = Q_2 - 1$.

For our simulations, we employ the aligned spin waveform model IMRPhenomD_NRTidalv2 [37]. Unlike in [37], our model contains amplitude tidal corrections and higher-order spin-squared and spin-cubed terms at 3.5 PN along with their corresponding spin-induced quadrupole moments, in addition to the spin-induced quadrupole moment terms at 2 PN and 3 PN. We simulate 120 sources in random noise realizations. The component masses lie between 1.0 $M_\odot$ and 2.0 $M_\odot$. Their tidal deformabilities are computed assuming the ALF2 EOS [38], which is a hybrid EOS with the variational-method APR EOS for nuclear matter [39] transitioning to color-flavor-locked quark matter. ALF2 has been picked since it is in agreement with recent multimessenger constraints on the EOS [11]. The sources are distributed uniformly in comoving volume between 15 and 150 Mpc with randomly chosen inclination angles and random sky locations. The dimensionless spin components are distributed uniformly between −0.5 and 0.5; while these values are significantly larger than observed in BNS systems, neutron stars not bound in BNS systems can rotate very rapidly, e.g., PSR J1807 − 2500B with a rotation frequency of 239 Hz [40,41]. Furthermore, the recent observation of GW190425 [14] whose estimated individual masses under the assumption of a BNS system (see Refs. [42,43] for possibility of the source being a neutron star-black hole binary) are inconsistent with the population of observed galactic BNSs showed that an extrapolation from our limited number of known galactic BNS systems is unreliable so that we include also higher spins in our investigation. However, we point out that this is an *ad hoc* choice considering that no millisecond pulsar has been observed inside a BNS system. We consider two injection sets for our simulated sources: (i) one where the injected quadrupole-monopole moments computed from the quasiuniversal relation in Eq. (1), i.e., $Q_{\rm injection} = Q_{\rm Yagi-Yunes}$, and (ii) one where the injected quadrupole-monopole moments do not follow the quasiuniversal relation; the injected moments here are half the values computed from Eq. (1) as an arbitrary choice of a modified quasiuniversal relation, i.e., $Q_{\rm injection} = 1/2 \times Q_{\rm Yagi-Yunes}$. Modified relations may occur in alternate theories of gravity like the dynamical Chern-Simons theory [44]; cf. e.g., [32]. In both kinds of injections, the quadrupole moments dQ_i are sampled uniformly between [0, 30] and the tidal deformabilities Λ_i are sampled uniformly between [0, 5000]. As for the other parameters, we sample the chirp mass uniformly between 0.7 $M_\odot$ and 2 $M_\odot$, the mass ratio m_2/m_1 is sampled uniformly between $1/8$ and 1, and the spin components are sampled uniformly between $[-0.7, 0.7]$. In this study, we assume Eq. (1) to be correct although there are associated errors at or below the percent level as discussed in Ref. [32]. In addition, use of the hybrid equation of state ALF2 may further introduce systematic errors.

III. RESULTS

A. Testing existing quasiuniversal relations

Based on the methods discussed before, we extract from our simulated BNS population the individual tidal deformabilities of the two stars (Λ_1 and Λ_2) and the spin-induced quadrupole moments Q_1 and Q_2. As an example, we show the recovery of one injection in Fig. 1. For the shown example, the injected values of $Q_{1,2}$ are determined from Eq. (1), i.e., we assume the correctness of the theoretically

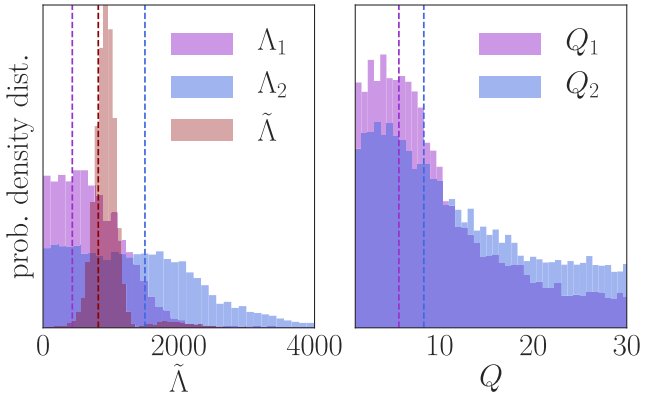

FIG. 1. Posterior probability distributions of Λ_1, Λ_2, $\tilde{\Lambda}$, Q_1, Q_2 from our set of injections. This particular setup has a signal-to-noise-ratio of 33.45. The neutron star masses are $m_1 = 1.472653$, $m_2 = 1.185832$, the dimensionless spins are $\chi_1 = 0.496$, $\chi_2 = -0.072$. Employing the ALF2 EOS, the tidal deformabilities are $\Lambda_1 = 431$, $\Lambda_2 = 1501$. The injected values are shown as vertical dashed lines. In particular, due to the large spin of the primary object, this setup is one of the few cases for which the individual tidal deformabilities and quadrupole moments can be determined with the advanced LIGO and advanced Virgo network.

derived quasiuniversal relations for the injection. We find that the vast majority of detections will not allow us to determine reliably the individual parameters $\Lambda_{1,2}$, $Q_{1,2}$. This is understandable since the individual parameters enter in the GW phase description in special combinations, e.g., tidal effects are dominated by the tidal deformability parameter

$$\tilde{\Lambda} = \frac{16}{13}\sum_{i=1,2}\Lambda_i \frac{m_i^4}{M^4}\left(12 - 11\frac{m_i}{M}\right), \tag{2}$$

see e.g., [45] and Fig. 1 for an illustration. Unfortunately, for the interpretation of quasiuniversal relations for single neutron stars, we have to measure accurately the parameters of the individual stars.

In Fig. 2 (top panel), we show all 240 recovered values, for both components of Q_i and Λ_i, together with their 1σ-credible interval, where we point out that in particular the lower bound on the tidal deformabilities and quadrupole moments are partially driven by the choice of our prior, i.e., that $\Lambda_i \geq 0$ and $Q \geq 1$. Simulations whose individual parameters return the prior are shown as faded. Only a few simulations have large enough signal-to-noise ratios as well as high individual spins so that about 15 out of a total of 240 individual parameters can be measured reliably. Among these sources, the lowest component spin is ~ 0.2. In almost all of these cases, these parameters belong to the more massive star in the binary system since its tidal deformability and spin-induced quadrupole moment dominate.

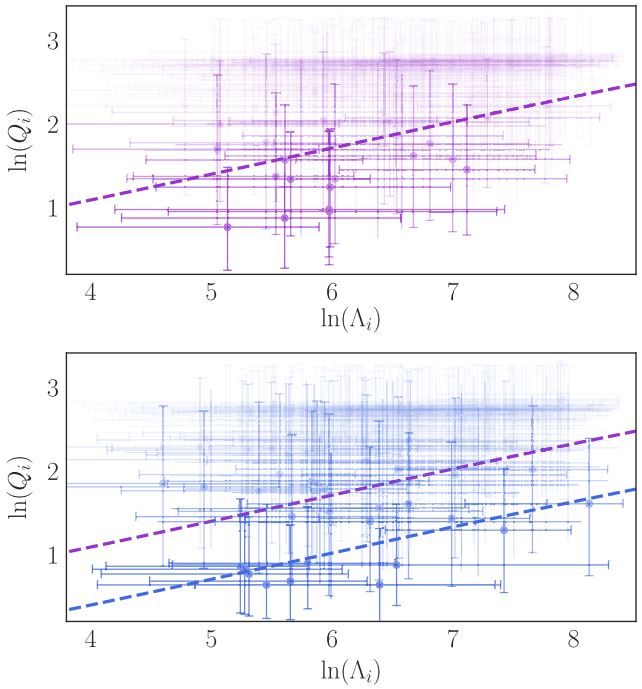

FIG. 2. Recovered $\Lambda_{1,2}$ and $Q_{1,2}$ values from our simulated population of 120 BNS systems for a 2G detector network. The shown error bars mark the 1σ-credible interval, while the individual markers refer to the 50% percentile. Fainter crosses refer to data with larger uncertainties. Top panel: the injection set based on the quasiuniversal relation Eq. (1). The dashed line refers to the quasiuniversal relation predicted by Yagi and Yunes, Eq. (1). Bottom panel: the dashed purple line refers to the Yagi-Yunes quasiuniversal relation, the blue dashed line the modified relation where Q is reduced by 50% with respect to Eq. (1), i.e., to the values used for the injection set.

For all systems for which Q_i can be measured, the predicted quasiuniversal relation connecting $Q - \Lambda$ lies within the 1σ-credible interval, which shows that, in principle, an assessment of the robustness of Eq. (1) is possible.

B. Probing new $\Lambda - Q$ relations

To answer the question if we would be able to detect a violation of Eq. (1), we have analyzed the same set of injections, i.e., identical parameters except for a reduction of the quadrupole moments $Q_{1,2}$ by 50%. We show the recovered parameters in Fig. 2 (bottom panel). As before, most of the simulations do not allow a reliable extraction of the quadrupole moments and the individual tidal deformabilities; however, for systems which are highly spinning and are located at a smaller distance, we find a set of data which are not in agreement with the Eq. (1) (purple line), but with the modified relation for which $Q_{\rm new} = Q/2$. Obviously, the particular choice of $Q_{\rm new}$ is arbitrary; however, it shows that large enough deviations from existing theoretical predictions might already be measurable with the second generation (2G) GW detectors [46].

C. Construction of $\Lambda - Q$ relations with 3G detectors

Finally, we simulate these sources in noise generated with envisaged sensitivities of future third generation (3G) detectors. For the 3G detectors, we use the noise curve of the Einstein Telescope (ET) detector with its ET-D configuration [47], a cryogenic detector to be built underground within the next decade in Europe [48], referred to as "ET." Reference [49] introduced the idea of an interferometer available within similar timelines in the United States, also known as "Cosmic Explorer" (CE). Unlike ET, CE is planned to be a ground-based detector with an arm length of 40 km. For our configuration, we choose a detector network including the ET detector, with its xylophone configuration (located at the Virgo site) and two CE-type detectors (located at the two LIGO sites) [50]. The 3G detectors will have the ability to reach lower cutoff frequencies of $f_{\rm low} \sim 1$ Hz, which means that sources like those considered before, i.e., for 2G detector network, will spend many more cycles in the 3G detectors' band, therefore improving both the signal-to-noise ratio as well as the duration for which the signal is visible in band. Due to limited computational resources, we keep the lower frequency cutoff with the 3G detectors same as the simulations with design sensitivity of advanced LIGO and advanced Virgo, i.e., $f_{\rm low} = 28$ Hz. While this means that we are not using the full potential of the future detectors and that we artificially reduce the maximum SNR [52], this procedure leads to a conservative result, i.e., the result will be better with future data-analysis techniques.

Employing the 3G network described above, we present the extracted values of Λ_i and Q_i for our two injection sets in Fig. 3, where we restrict to using the data for which (i) $\ln(Q) \leq 2.5$, larger values are basically not expected and an indicator that the prior is recovered and (ii) we remove all data points for which $\Delta \ln(Q) > 1$, where $\Delta \ln(Q)$ refers to the width of the 1σ-credible interval in the log-log plot, Fig. 3. We find clearly that the recovered source parameters cluster around the respective, injected quasiuniversal relations.

For a quantitative measure, we try to extract a phenomenological $Q - \Lambda$ relations directly from our recovered data set. We fit the data points shown in Fig. 3 according to

$$\ln Q = \hat{a}_i + \hat{b}_i \ln \Lambda. \tag{3}$$

For the fitting, we use weights that are indirectly proportional to the size of the 1σ-credible interval of Q_i, i.e., setups in which the induced quadrupole moment is measured more accurately are favored. Different to Eq. (1) we decided to remove higher-order terms since the measurement uncertainties do not allow any reliable determination of terms $\propto \ln(\Lambda)^k$ with $k > 1$. We find $\hat{a} = -0.05014$, $\hat{b} = 0.2595$ with a residual of 0.32 for the data set shown in the top panel, i.e., those simulations employing the Yagi-Yunes relation, and $\hat{a} = -1.348$, $\hat{b} = 0.357$ for our modified quasiuniversal relation with a residual of 0.26. The residuals of the individual fits are incorporated via the thin dashed green lines and emphasize again that with 3G detectors it might be possible to distinguish between different Q – Λ relations.

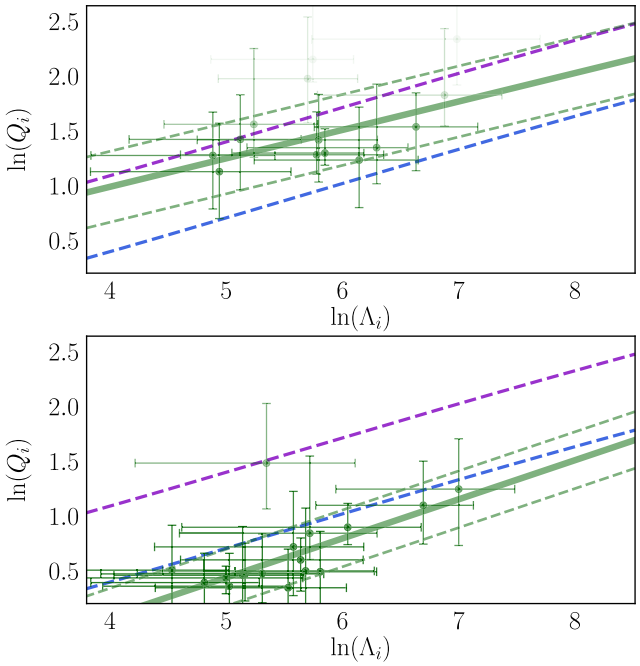

FIG. 3. Recovered $\Lambda_{1,2}$ and $Q_{1,2}$ values from our simulated population of 120 BNS systems for which $\ln(Q_i) < 2.5$ and $\Delta \ln(Q) < 1$ for a 3G detector network. The shown error bars ($\Delta \ln \Lambda$) mark the 1σ-credible interval. Fainther crosses refer to data with larger uncertainties. The dashed purple line refers to Eq. (1), the blue dashed line to the quasiuniversal for which Q_i got reduced by 50%, and the green solid line refers to the best fit of the data, where thin dashed green lines mark the residual of the fit. Top panel: hte injection set is based on Eq. (1). Bottom panel: the injection set is based on our modified quasiuniversal relation.

IV. CONCLUSION

We have tested if future GW detections might allow us to extract phenomenological relations between the spin-induced quadrupole moment and the tidal deformability of individual neutron stars. For this purpose, we have studied a simulated population of 120 BNS systems for a 2G detector network and a 3G detector network.

We find that at design sensitivity a reduction of 50% in the quadrupole moment would be visible; we anticipate that smaller deviations might not be observable. However, this means that Advanced LIGO and Advanced Virgo might be able to detect possible deviations from existing, theoretically predicted, quasiuniversal relations. However, one would need a 3G detector network for a more reliable measurement. We find that with a network of 2 Cosmic Explorer-like detectors and 1 Einstein Telescope, we might be able to extract quasiuniversal relations from the neutron star properties inferred from the analysis of the gravitational wave signals.

In the hypothetical scenario, in which the extracted quasiuniversal relations are not in agreement with theoretical predictions, this would either indicate a violation of general relativity or that our current description of the interior of neutron stars is insufficient.

ACKNOWLEDGMENTS

We thank Sebastian Khan and the LIGO-Virgo Collaborations' extreme matter group for helpful discussions. We thank N. V. Krishnendu and Nathan K. Johnson-McDaniel for helpful feedback on the paper and going through it carefully. We also thank Nathan K. Johnson-McDaniel and An Chen for support setting up the 3G injections. A. S. and T. D. are supported by the research programme of the Netherlands Organisation for Scientific Research (NWO). T. D. acknowledges support by the European Union's Horizon 2020 research and innovation program under Grant No. 749145, BNSmergers. The authors are grateful for computational resources provided by the LIGO Laboratory and supported by the National Science Foundation Grants No. PHY-0757058 and No. PHY-0823459.

[1] B. P. Abbott *et al.* (Virgo and LIGO Scientific Collaborations), Phys. Rev. Lett. **119**, 161101 (2017).
[2] B. Abbott *et al.* (LIGO Scientific and Virgo Collaborations), Phys. Rev. Lett. **121**, 161101 (2018).
[3] B. P. Abbott *et al.* (LIGO Scientific and Virgo Collaborations), Phys. Rev. X **9**, 011001 (2019).
[4] E. Annala, T. Gorda, A. Kurkela, and A. Vuorinen, Phys. Rev. Lett. **120**, 172703 (2018).
[5] C. D. Capano, I. Tews, S. M. Brown, B. Margalit, S. De, S. Kumar, D. A. Brown, B. Krishnan, and S. Reddy, Nat. Astron. (2020).
[6] A. Bauswein, O. Just, H.-T. Janka, and N. Stergioulas, Astrophys. J. **850**, L34 (2017).
[7] D. Radice, A. Perego, F. Zappa, and S. Bernuzzi, Astrophys. J. **852**, L29 (2018).
[8] S. De, D. Finstad, J. M. Lattimer, D. A. Brown, E. Berger, and C. M. Biwer, Phys. Rev. Lett. **121**, 091102 (2018); **121**, 259902(E) (2018).
[9] B. Margalit and B. D. Metzger, Astrophys. J. **850**, L19 (2017).
[10] E. R. Most, L. R. Weih, L. Rezzolla, and J. Schaffner-Bielich, Phys. Rev. Lett. **120**, 261103 (2018).
[11] M. W. Coughlin *et al.*, Mon. Not. R. Astron. Soc. **480**, 3871 (2018).
[12] D. Radice and L. Dai, Eur. Phys. J. A **55**, 50 (2019).
[13] T. Dietrich, M. W. Coughlin, P. T. Pang, M. Bulla, J. Heinzel, L. Issa, I. Tews, and S. Antier, arXiv:2002.11355.
[14] B. P. Abbott *et al.* (LIGO Scientific and Virgo Collaborations), Astrophys. J. Lett. **892**, L3 (2020).
[15] M. W. Coughlin *et al.*, Astrophys. J. **885**, L19 (2019).
[16] M. W. Coughlin, T. Dietrich, S. Antier, M. Bulla, F. Foucart, K. Hotokezaka, G. Raaijmakers, T. Hinderer, and S. Nissanke, Mon. Not. R. Astron. Soc. **492**, 863 (2020).
[17] J. B. Hartle, Astrophys. J. **150**, 1005 (1967).
[18] W. G. Laarakkers and E. Poisson, Astrophys. J. **512**, 282 (1999).
[19] G. Pappas and T. A. Apostolatos, Phys. Rev. Lett. **108**, 231104 (2012).
[20] E. Poisson, Phys. Rev. D **57**, 5287 (1998).
[21] I. Harry and T. Hinderer, Classical Quantum Gravity **35**, 145010 (2018).
[22] A. Samajdar and T. Dietrich, Phys. Rev. D **100**, 024046 (2019).
[23] M. Agathos, J. Meidam, W. Del Pozzo, T. G. F. Li, M. Tompitak, J. Veitch, S. Vitale, and C. Van Den Broeck, Phys. Rev. D **92**, 023012 (2015).
[24] N. V. Krishnendu, K. G. Arun, and C. K. Mishra, Phys. Rev. Lett. **119**, 091101 (2017).
[25] N. V. Krishnendu, M. Saleem, A. Samajdar, K. G. Arun, W. Del Pozzo, and C. K. Mishra, Phys. Rev. D **100**, 104019 (2019).
[26] K. Yagi and N. Yunes, Science **341**, 365 (2013).
[27] Z. Carson, K. Chatziioannou, C.-J. Haster, K. Yagi, and N. Yunes, Phys. Rev. D **99**, 083016 (2019).
[28] D. D. Doneva, S. S. Yazadjiev, N. Stergioulas, and K. D. Kokkotas, Astrophys. J. **781**, L6 (2013).
[29] B. Haskell, R. Ciolfi, F. Pannarale, and L. Rezzolla, Mon. Not. R. Astron. Soc. **438**, L71 (2014).
[30] N. Andersson and P. Pnigouras, arXiv:1905.00012.
[31] N. Andersson and P. Pnigouras, Phys. Rev. D **101**, 083001 (2020).
[32] K. Yagi and N. Yunes, Phys. Rev. D **88**, 023009 (2013).
[33] J. Veitch *et al.*, Phys. Rev. D **91**, 042003 (2015).
[34] LIGO Scientific Collaboration, LIGO Algorithm Library–LALSuite, free software (GPL) (2018).
[35] J. Veitch and A. Vecchio, Phys. Rev. D **81**, 062003 (2010).
[36] J. Skilling, Bayesian Anal. **1**, 833 (2006).
[37] T. Dietrich, A. Samajdar, S. Khan, N. K. Johnson-McDaniel, R. Dudi, and W. Tichy, Phys. Rev. D **100**, 044003 (2019).
[38] M. Alford, M. Braby, M. W. Paris, and S. Reddy, Astrophys. J. **629**, 969 (2005).
[39] A. Akmal, V. R. Pandharipande, and D. G. Ravenhall, Phys. Rev. C **58**, 1804 (1998).
[40] D. R. Lorimer, Living Rev. Relativity **11**, 8 (2008).
[41] J. M. Lattimer, Annu. Rev. Nucl. Part. Sci. **62**, 485 (2012).
[42] K. Kyutoku, S. Fujibayashi, K. Hayashi, K. Kawaguchi, K. Kiuchi, M. Shibata, and M. Tanaka, Astrophys. J. **890**, L4 (2020).
[43] M.-Z. Han, S.-P. Tang, Y.-M. Hu, Y.-J. Li, J.-L. Jiang, Z.-P. Jin, Y.-Z. Fan, and D.-M. Wei, Astrophys. J. **891**, L5 (2020).
[44] S. Alexander and N. Yunes, Phys. Rep. **480**, 1 (2009).

[45] E. E. Flanagan and T. Hinderer, Phys. Rev. D **77**, 021502 (2008).
[46] We expect that this observation does not depend on the particular EOS, but that only the deviation from Eq. (1) is important.
[47] S. Hild *et al.*, Classical Quantum Gravity **28**, 094013 (2011).
[48] M. Punturo *et al.*, Classical Quantum Gravity **27**, 194002 (2010).
[49] S. Dwyer, D. Sigg, S. W. Ballmer, L. Barsotti, N. Mavalvala, and M. Evans, Phys. Rev. D **91**, 082001 (2015).
[50] We note that we include an older CE noise curve and that we do not take a frequency-dependent response into account. We expect that due to our relatively large initial frequency, the effect of the frequency dependence of the response function is small. We refer the reader to [51] for additional details.
[51] A. Chen, N. K. Johnson-McDaniel, T. Dietrich, and R. Dudi, Phys. Rev. D **101**, 103008 (2020).
[52] Although we use a $f_{\rm low} = 28$ Hz for the 3G network, we obtain SNR values of about 10^2 up to 10^3, i.e., about 20–30 times larger than for the 2G network.